CFD-based mapping of the thermo-acoustic stability of a laminar premix burner

By R. Kaess†, W. Polifke†, T. Poinsot‡, N. Noiray¶, D. Durox‖, T. Schuller‖ AND S. Candel‖

A novel method for thermo-acoustic stability analysis is presented and validated against experimental data from a laminar premix combustion test rig. The method combines CFD simulation of compressible, reacting flow with a low-order network model to identify the open-loop transfer function of the test rig. The linear growth rates of stable as well as unstable eigenmodes are then evaluated from a Nyquist plot. Using times series data from only one CFD run, the stability map of the test rig, i.e., the dependence of stability and frequency of the eigenmodes modes on the plenum length, is reproduced successfully in this study.

1. Introduction

Thermo-acoustic instabilities are a cause for concern in combustion applications as diverse as small household burners, gas turbines or rocket engines. Because the numerical modeling of this multi-physics, multi-scale phenomenon is very challenging, efficient strategies of *divide and conquer* have been developed to predict such instabilities (see, e.g., Lieuwen & Yang 2006, or Polifke 2007). Typically, a reduced model of the flame dynamics is combined with a linearized description of (acoustic) wave propagation in the combustor. For the latter, low-order "network models" have been popular for a long time; finite-volume or finite-element based tools have been developed more recently. The flame is usually regarded as a *single-input, single-output* (SISO) element and described by a flame-transfer function

$$F(\omega) = \frac{\hat{\dot{Q}}(\omega)/\bar{\dot{Q}}}{\hat{u}/\bar{u}}, \tag{1.1}$$

which gives the response of the heat release rate $\dot{Q}$ to a perturbation of the velocity u upstream of the flame.

Such an approach may be suitable, e.g., for an acoustically compact lean premix swirl flame in the combustor of a stationary gas turbine (see Fig. 1, left). Consider, however, a typical aero-engine combustor. Here the flame extends over a considerable fraction of the combustor length, i.e., there is no local coupling between heat release and acoustics. Furthermore, the momentary heat release rate will be influenced by fluctuations of both primary and secondary air injection mass flow rates, i.e., the flame represents a *multiple input* system. The topology of the combustor, with secondary and cooling air injection holes distributed along the liner, makes it difficult to model acoustic wave propagation and dissipation.

† Thermodynamik, TU München
‡ CERFACS, Toulouse
¶ Alstom Power, Baden
‖ EM2C, École Centrale Paris

FIGURE 1. Combustor of a stationary gas turbine (left) and an aero-engine (right).

For such situations, Kopitz & Polifke (2008) have recently proposed a novel hybrid "CNN" approach: Combining **C**omputational fluid dynamics with low-order **N**etwork modeling, the open-loop transfer function of the combustion system is computed. Eigenmodes and the stability characteristics are then deduced from a **N**yquist plot. Explicit knowledge of the frequency response or the transfer matrix of the heat source is not required. Provided that the CFD model is sufficiently powerful, aero-acoustic and thermo-acoustic interactions can be represented with high accuracy.

Kopitz & Polifke (2008) have established proof of concept for CNN by validation against a simple, semi-analytical model of a Rijke tube. In the present work, the method is used to generate the stability map of a laminar, premix, perforated-plate burner. Results obtained are compared with experimental data obtained from a laminar, premix perforated-plate burner.

2. Test rig setup and experimental results

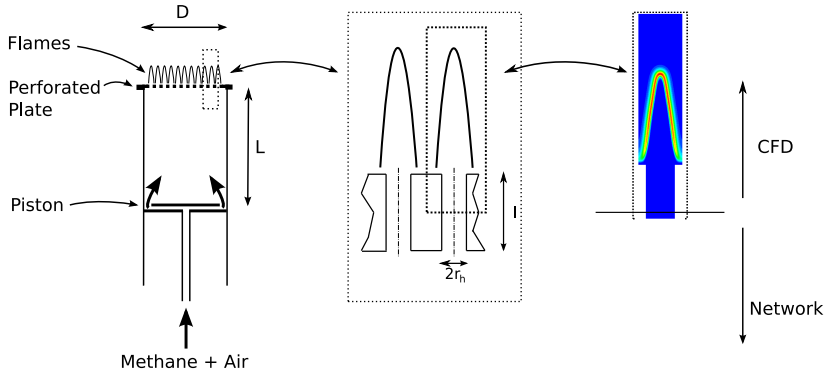

FIGURE 2. Sketch of the burner test rig with details of the perforated-plate geometry (middle) and CFD domain (right).

The burner test rig which serves as a validation in this work has been examined by the group at EM2C / Ecole Centrale Paris (Noiray 2007; Noiray *et al.* 2007, 2008). The rig (see Fig. 2) consists of a cylindrical tube closed by a perforated plate at the top. A movable piston is located at the opposite end of the tube such that the plenum length L is variable. The perforated plate serves as a flame holder for a multitude of laminar, conical, unconfined flames, which burn just above the perforated plate. The effect of plate geometry (thickness, size and number of holes) and plenum length L on combustion dynamics has been investigated in systematic studies by Noiray *et al.* (2007, 2008). For the current work, only "Plate 4" with thickness $l = 30\,\text{mm}$, radius $r_h = 1\,\text{mm}$ and 420 holes is used. Other important parameters of the setup are: pipe diameter $D = 70\,\text{mm}$,

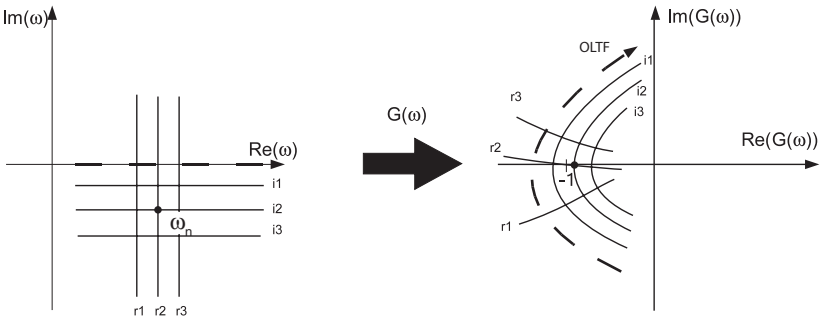

FIGURE 3. The Nyquist curve (dotted line in the right plot) is the image of the positive half of the real axis in the ω-plane under the OLTF mapping $\omega \to G(\omega)$. Case shown corresponds to an unstable eigenfrequency with $\Im(\omega) < 0$.

length $L = 0.09 - 0.75\,\mathrm{m}$, equivalence ratio $\phi = 0.86$ and mass flow rate $\dot{m} = 5.4\,\mathrm{g/s}$. The burner is operated using a methane-air mixture. A stability map for this configuration is shown in Fig. 11. Noiray *et al.* also performed measurements of the flame response to upstream flow perturbations, using OH^- chemiluminescence for the heat release rate and LDA for the velocity. Both the linear response ("flame transfer function", see Fig. 9) and the non-linear response ("flame describing function") were measured, the latter was used to determine limit cycle amplitudes and non-linear instabilities for various plate geometries. In doing so, it was assumed that the flame response does not vary with plate thickness. For a complete description of the configurations investigated and results achieved to date, the reader is referred to the publications of Noiray *et al.* (2007a, 2007b, 2008).

3. CFD-based generation of Nyquist plots for thermo-acoustic stability analysis

The use of concepts and tools from control theory for the analysis of thermo-acoustic combustion instabilities goes back to the 1970s (see, e.g., Baade 1974). These early studies were limited to simple combustor geometries in the limit of low frequencies ("Helmholtz-mode").

Polifke and co-workers have shown how the equivalent of the open-loop transfer function $G(\omega)$ can be generated in the general case from a linear, low-order network model of thermo-acoustic interactions (Polifke *et al.* 1997; Sattelmayer & Polifke 2003*a*,*b*). From the open-loop transfer function (OLTF), a Nyquist plot is generated, frequencies and growth / decay rates of both unstable and stable eigenmodes can then be inferred "by inspection" from the Nyquist plot. To do so, one considers the image curve of the positive half of the real axis $\omega = 0 \to \infty$ under the OLTF mapping in the $G(\omega)$-plane, as shown in Fig. 3. The OLTF is constructed such that each eigenfrequency ω_n is mapped to the "critical point" -1 in the image plane, i.e., $G(\omega) = -1$. It follows that as one moves along the Nyquist curve in the direction of increasing frequency ω, an eigenmode with eigenfrequency ω_n is encountered each time the Nyquist curve passes the critical point -1. In Fig. 3, only one sweep past an eigenfrequency is shown. If the critical point lies to the right of the Nyquist curve (orientation is defined by the direction of propagation along the Nyquist curve), the eigenfrequency ω_n lies in the lower half ω-plane. It follows that the corresponding n-th eigenmode is unstable, because a negative imaginary part of an eigenfrequency ω_n implies growth of the mode (with convention $\exp(i\omega t)$ for the time dependence). On the other hand, if the critical point is located to the left, the eigen-

mode is stable, while the mode is neutrally stable if the Nyquist curve passes through the critical point.

The real part of an eigenfrequency ω_n is determined as the frequency $\omega_n^+ \in \mathbb{R}$ at which the Nyquist curve attains closest proximity to the critical point, i.e., the function $|G(\omega)+1|$ reaches a local minimum. The imaginary part $\Im(\omega_n)$ or equivalently the growth rate Γ_n of the nth eigenmode can be computed from the scaled distance of the Nyquist curve from the critical point -1,

$$\Gamma \equiv \exp\left\{-2\pi\frac{\Im(\omega)}{\Re(\omega)}\right\} - 1 = \left\{\pm 2\pi\frac{|G(\omega_n^+)+1|}{\sigma_n\,\omega_n^+}\right\} - 1, \tag{3.1}$$

with a "+"- sign on the r.h.s. for an unstable mode and a "−"- sign for a stable mode. Details on the scaling factor σ_n are given in Appendix C of Kopitz & Polifke (2008). This method of identifying eigenmodes and their stability is based on the assumption that the mapping $\omega \to G(\omega)$ is *conformal*† in the neighborhood of each eigenfrequency ω_n. This point will be addressed again later.

As discussed in the Introduction, combustor configurations of technical interest are often not amenable to the established *divide and conquer* modeling strategies. For such situations, Kopitz & Polifke (2008) have proposed to determine the OLTF of a combustion system with the hybrid CNN approach, which combines CFD data with a low-order network model: The network model is used for elements like the air supply or a chimney, for which a low-order description of acoustic wave propagation is known. The CFD model, on the other hand, represents only those elements of the combustion system for which a network-formulation is not suitable (or not known), e.g., the flame. Further scenarios for the use of CNN and expected advantages are discussed by Kopitz & Polifke (2008).

For the test rig of Noiray *et al.*, the obvious CNN model setup is to represent the upstream plenum and possibly a part of the perforated plate by a low-order model for 1-D wave propagation, while the CFD domain is restricted to a very small part of the test rig, i.e., the flame stabilized above one hole of the perforated plate (see Fig. 2). Following the procedure proposed by Kopitz & Polifke (2008), a broad-band acoustic excitation of an ingoing characteristic wave amplitude f is imposed at the upstream boundary of the computational domain. Scattering of acoustic waves and the response of the flame to the perturbation generates an outgoing wave g. From the computed time series f_c and g_c at a monitor plane close to the inlet, a response function

$$H(\omega) \equiv \frac{\hat{g}_c}{\hat{f}_c} \tag{3.2}$$

is derived with correlation analysis (also called "Wiener-Hopf inversion", see Polifke *et al.* 2001; Polifke 2004). It is emphasized that the response function $H(\omega)$ is neither the flame response function F as defined in Eq. (1.1), nor the OLTF $G(\omega)$ of the combustion system. The latter is obtained from the network model for the sections upstream of the CFD domain, with the response function H computed from the CFD subdata as input.

When applying the CNN method to the perforated-plate burner of EM2C, one could place the "cut", i.e., the interface between the CFD and the low-order submodels, respectively, inside the plenum, or inside the perforated plate. If the cut is placed in the plenum,

† If U is an open subset of the complex plane $\mathbb{C}$ and $f : U \to \mathbb{C}$ an analytical function in U, then f is *conformal* if and only if it is *holomorphic* (complex-differentiable) and $f'(z) \neq 0$ on U. This implies that the function f is infinitely often differentiable and can be described by its Taylor series in a neighborhood of each point in its domain.

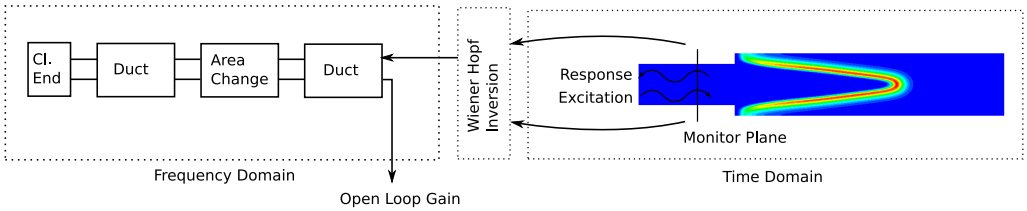

FIGURE 4. Coupling between network model and CFD using correlation analysis

the CFD domain obviously includes part of the plenum and the complete flow passage inside the plate. This has the advantage that scattering and dissipation of acoustic waves in these sections will be described by the CFD model with high accuracy; low-order modeling is limited to reflection of acoustic waves at the piston (a "closed end" with $f = g$) and wave propagation in the plenum.

On the other hand, for plates like "Plate 4" investigated in this work with thickness $l = 30\,\mathrm{mm}$, the compute resources required to model the flow in the plenum and the plate will be quite significant. Also, preliminary low-order modeling suggested that placing the "cut" inside the plate reduces problems with resonant excitation of the CFD submodel and singularity of the OLTF. This is discussed in the next section. Furthermore, with the "cut" in the plate (and assuming that the flame response does not vary with plate thickness), it is possible in principle to study the effect of varying plate thickness on the stability behavior based on data from only one CFD run. It has therefore been decided to place the "cut" inside the perforated plate, just 2 mm away from the downstream face. The network model comprises then the following elements: the "closed end" acoustic boundary at the piston, the plenum with wave propagation in both directions (the "duct" in Fig. 4), the flow contraction into the holes of the perforated plate ("area change"), where incoming acoustics waves are scattered and the holes of the plate up to the "cut" (again a duct element).

The test rig considered here is well amenable to "standard" low-order network modelling, once the flame transfer function $F(\omega)$ is determined from experiment (or with CFD/SI, see Polifke *et al.* 2001). This has been demonstrated by Noiray *et al.* (2007, 2008). Therefore the perforated-plate burner is not a typical example of a configuration for which the CNN method has been conceived – it is, in a sense, too simple. However, in the context of a validation study, this simplicity is an advantage, as it facilitates analysis and interpretation of results.

4. Low-order modeling

As is often the case with thermo-acoustic combustion instabilities, low-order modelling provides useful insight into the problem under investigation. Some results are summarized in this section.

4.1. *Flame-transfer function*

The flame frequency response measured by Noiray (2007) can be fitted with good accuracy to the following functional form:

$$F(\omega) = (1+a)e^{-i\omega\tau_1-\frac{\omega^2\sigma_1^2}{2}} - ae^{-i\omega\tau_2-\frac{\omega^2\sigma_2^2}{2}}. \tag{4.1}$$

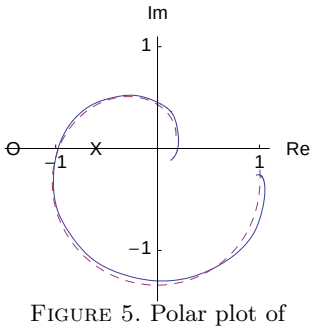

FIGURE 5. Polar plot of flame-transfer function $F(\omega)$.

Such a formulation with two time-delays and dispersion has been used previously by Gentemann & Polifke (2007). Using a non-linear fitting routine, the following parameter values have been determined to give good agreement with the experimental data presented in Fig. 7.2 of the dissertation of Noiray (2007): $a = 0.906$, $\tau_1 = 0.912$ ms, $\sigma_1 = 0.334$ ms, $\tau_2 = 0.122$ ms, $\sigma_2 = 0.817$ ms. In Fig. 5, the continuous line shows the experimental data for $F(\omega)$ for frequencies up to 1000 Hz, while the dashed line represents the fit to Eq. (4.1). Note that the experimental data were obtained with a low level of forcing $u'_{rms}/\bar{u} = 0.09$ and represent the linear flame response.

4.2. *Transfer matrix of plate and flame*

The most interesting acoustic elements are obviously the perforated plate and the flame stabilized above it. The following low-order representation of these elements is used:

$$\mathbf{T} = \underbrace{\begin{pmatrix} \xi & 0 \\ 0 & (1+\Theta F)/\alpha \end{pmatrix}}_{\text{Flame}} \underbrace{\begin{pmatrix} 1 & -ikl_p \\ 0 & \alpha \end{pmatrix}}_{\text{Perf. Plate}} = \begin{pmatrix} \xi & -i\xi k l_p \\ 0 & 1+\Theta F \end{pmatrix}. \tag{4.2}$$

Here, $\mathbf{T}$ is the transfer matrix for variables $(p'/\rho c, u')$ on the up- and downstream side, respectively. $\xi \equiv \rho_c c_c/\rho_h c_h$ is the ratio of specific impedances in the upstream side (subscript c for "cold") and the downstream "hot" side of the element, $\Theta \equiv T_h/T_c - 1 = \xi^2 - 1$ is the temperature excess and $\alpha \equiv A_{\text{Perforation}}/A_{\text{Plenum}}$ the ratio of total cross-sectional area of perforated plate and plenum (the *porosity* of the plate). For pressure coupling across the plate, we have followed Noiray *et al.* (2007, 2008) and assumed $\Delta p' = -i\omega\rho_c l_p u'$ with a factor l_p that introduces some viscous damping due to a Stokes boundary layer:

$$l_p \equiv l\left(1 + \frac{l_\nu}{r_p}(1+i)\right) \text{ with Stokes length } l_\nu \equiv \sqrt{2\nu/\omega}. \tag{4.3}$$

4.3. *Response calculations*

As discussed in the previous section, the purpose of the CFD simulation is to generate the response function $H(\omega) = \hat{g}_c/\hat{f}_c$, relating amplitude and phase of the excitation signal $\hat{f}_c$ and the outgoing wave amplitude $\hat{g}_c$ at the "cut" of the hybrid model, i.e., at the interface between the CFD and the low-order submodels, respectively. For a comparatively simple combustion system like the one at hand, the response function $H(\omega)$ can be estimated also from a low-order model.

For the first configuration analyzed, the "cut" is located in the plenum, some distance l_c upstream of the plate. If the transfer matrix $\mathbf{T}$ introduced in Eq. (4.2) is converted into the scattering matrix $\mathbf{S}$ (see Gentemann & Polifke 2007), an analytical expression for the response function is obtained:

$$H(\omega) = e^{-2ikl_c}\mathbf{S}_{21}(\omega) = e^{-2ikl_c}\frac{1+\Theta F(\omega) - \xi(1-ikl_p)}{1+\Theta F(\omega) + \xi(1-ikl_p)}. \tag{4.4}$$

The significance of this result is the following: Obviously the response $H(\omega)$ depends on frequency through the factors containing the wavenumber $k = \omega/c$ or the flame frequency response $F(\omega)$. If the gain $|H(\omega)|$ attains a large value for some frequencies, broad-band excitation of the system will cause correspondingly large amplitude oscillations of

velocity, pressure and heat release by *resonant excitation* (not self-excited instability). Large amplitudes can lead to deviation from linear behavior or to divergence of the computation, and should be avoided.

The response $H(\omega)$ as given by Eq. (4.4) will be large whenever the denominator of the scattering matrix coefficient $\mathbf{S}_{21}$ becomes small (see the corresponding discussion on scattering and generation of acoustic energy in Gentemann & Polifke 2007). For frequencies of order 500 Hz, the factor $ikl_p \ll 1$ and may be neglected; the condition for resonant excitation then simplifies to $1 + \Theta F + \xi = 0$ or

$$F(\omega) = -\frac{\xi + 1}{\Theta} = -\frac{1}{\xi - 1} \approx -0.625, \tag{4.5}$$

with a value of $\xi = 2.6$ for the present conditions.

Figure 5 indicates that the flame transfer function measured by Noiray (2007), although not passing through the point -0.625 (marked with an "X" in the figure), comes fairly close to that point for frequencies around 500 Hz, such that some resonant amplification of the excitation signal must be expected. As this is undesirable, a second setup for the CNN approach has been analyzed, with the "cut" located inside the perforated plate, such that the flow contraction from the plenum into the perforation and wave propagation within the perforation is part of the network submodel. For this configuration, one obtains the condition

$$F(\omega) = -\frac{\xi/\alpha + 1}{\Theta} \approx -1.4, \tag{4.6}$$

indicated by "O" in Fig. 5, for resonant amplification. Unfortunately, with the polar plot of the flame-transfer function crossing the real axis just between points "X" and "O", we may not expect that the setup with the "cut" inside the plate yields a response curve with significantly reduced resonant peaks. This conclusion would not be so if the flame response $F(\omega)$ showed more noticeable reduction in gain around 500 Hz (c.f. Fig. 9). Then the configuration with the "cut" inside the plate would be advantageous.

Note that a related problem is the occurrence of singularities in the OLTF $G(\omega)$. In the vicinity of a singularity, conformality of the mapping breaks down. Therefore, if a singularity of the OLTF is close to an eigenmode, it is not possible to read off that eigenfrequency from the Nyquist plot. Preliminary low-order modelling can be helpful in analyzing this scenario. However, due to lack of space these questions are not discussed further in this report.

4.4. *Area change and attenuation in the perforated plate*

In the course of this study it became apparent that the simple model of acoustic wave scattering and attenuation at the perforated plate expressed by Eq. (4.2) yielded a much stronger tendency for instability than was observed experimentally (see below). Therefore, more sophisticated low-order models for these elements were invoked. For the flow constriction into the plate

$$\begin{pmatrix} \frac{p'}{\rho c} \\ u' \end{pmatrix}_d = \begin{pmatrix} 1 & -ikl_{\text{eff}} - \zeta M \\ 0 & \alpha \end{pmatrix} \begin{pmatrix} \frac{p'}{\rho c} \\ u' \end{pmatrix}_u , \tag{4.7}$$

according to Polifke (2004), where M denotes the Mach number based on the volume flux, α the area ratio, ζ an acoustic loss coefficient and l_{eff} an effective length. The values $\zeta = 6$ and $l_{\text{eff}} = 7.64 \cdot 10^{-4}\,\text{m}$ were determined with CFD simulation and correlation analysis for these parameters.

To account for wave propagation and attenuation inside the porous plate

$$\begin{pmatrix} f \\ g \end{pmatrix}_d = \begin{pmatrix} e^{-i(k+\zeta_S)x} & 0 \\ 0 & e^{i(k+\zeta_S)x} \end{pmatrix} \begin{pmatrix} f \\ g \end{pmatrix}_u , \tag{4.8}$$

with a damping coefficient ζ_S to account for the effect of the Stokes boundary layer

$$\zeta_S = (1+i)\frac{\sqrt{2\omega\nu}}{2r_h c}\left(1+\frac{\gamma-1}{\mathrm{Pr}^{0.5}}\right). \tag{4.9}$$

5. CFD setup

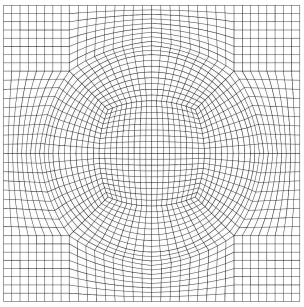

FIGURE 6. Front view of the mesh used for the computations.

The LES-solver AVBP developed by CERFACS, Toulouse, has been used for this work. The computational domain comprises a short part (length 5 mm) of one perforation and the flame stabilized above it (see Figs. 2 and 8). An axis-normal cut through the block-structured mesh is shown in Fig. 6. With a total of $n \approx 470,000$ cells, the flame front is resolved on more than 10 cells. A Wale LES-subgrid scale model is used, although the resolution of the grid is very close to a DNS. A Lax-Wendroff explicit time-stepping scheme with a fixed time step of $3.5e-8s$ is used. Typically, a total of 1.5 million time steps are calculated to generate the response function H. The combustion model is an Arrhenius-Law with one step chemistry for methane. Several monitor planes are placed along the axis in the numerical domain. They permit the extraction of surface averages of velocity, pressure, speed of sound and density. From these quantities, the characteristic wave amplitudes f and g are computed.

5.1. *Acoustic boundary conditions*

The inlet and the outlet boundary conditions are non-reflecting boundary conditions with wave masking as developed by Polifke *et al.* (2006), implemented by Kaess *et al.* (2008) in AVBP. A monitor plane close to the inlet provides the interface for the coupling with the network model (the "cut" in the hybrid model). The non-reflecting outlet boundary is imposed downstream of the flame. The simulation was excited with a low-pass filtered pseudo random binary signal (PRBS) (see Huber & Polifke 2009), imposed as an ingoing characteristic wave f with an amplitude of 2 % of the mean flow velocity. The lateral boundary conditions are symmetry conditions.

5.2. *Thermal boundary conditions*

The thermal boundary conditions used for the perforated plate are of particular interest because flame stabilization and dynamic flame response depend in a sensitive manner on the plate surface temperature and the heat loss to the plate (Rook *et al.* 2002). To simulate the interactions between heat transfer and heat release accurately, a conjugate heat transfer approach including heat conduction inside the plate and heat loss of the plate (by radiation and by the fuel/air mixture passing through the perforation) would be most appropriate. This was, however, not possible with the version of AVBP used for this work.

If one simply applies an adiabatic boundary condition, the absence of heat loss permits the flame to stabilize directly on the perforated plate, contrary to experimental

observation (Noiray *et al.* 2007, 2008). If instead the front side of the perforated plate is modeled as an isothermal wall with temperature T_W significantly below the adiabatic flame temperature T_{ad}, chemical reactions are quenched close to the plate and the flame stabilizes at a certain distance h above the plate (see Fig. 8).

The temperature T_W of the downstream side of the plate surface can be estimated by comparing the specific thermal resistances for heat transfer from the flame to the plate, and from the plate to the fuel/air mixture, respectively. For the latter, the plate is considered as a straight cooling fin with Nußelt number and heat-transfer coefficient α corresponding to developed pipe flow, i.e., Nu ≈ 4 and

$$\alpha = \frac{\mathrm{Nu}\,\lambda_{air}}{2r_h} = 52\frac{W}{m^2K}. \tag{5.1}$$

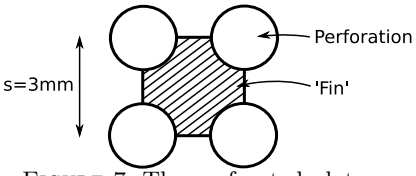

FIGURE 7. The perforated plate as "cooling fin".

Figure 7 shows the relevant geometrical parameters: the frontal area $A = s^2 - r_h^2\pi$, the "circumference" $U = 2r_h\pi$ and the extended surface area $M = \pi 2r_h l$. The dimensionless fin parameter μ, the heat flux $\dot{q}$ at the surface of the plate, and the specific thermal resistance R_{fin} of the plate surface are calculated using standard formulas for straight fins.

With $l = 30\,\mathrm{mm}$ for the thickness of "Plate 4" and $\lambda_d = 15\,\mathrm{W/(mK)}$ for stainless steel, the following is obtained:

$$\mu = \sqrt{\frac{\alpha U l^2}{A\lambda_d}} \approx 1.8, \tag{5.2}$$

$$\dot{q} = \frac{\sqrt{\alpha\lambda_s AU}}{A}\tanh(\mu)\Delta T, \tag{5.3}$$

$$R_{\mathrm{fin}} \equiv \frac{\Delta T}{\dot{q}} = \frac{A}{\sqrt{\alpha\lambda_d AU}}\frac{1}{\tanh(\mu)} \approx 1.16\cdot 10^{-3}\,\frac{m^2K}{W}. \tag{5.4}$$

Neglecting convection, the specific thermal resistance R_h for the heat flux from the flame tip to the perforated plate is estimated from the stand-off distance $h \approx 1\,\mathrm{mm}$ of the flame and the heat conductance of air $\lambda_{air} = 0.026\,\mathrm{W/mK}$:

$$R_h = \frac{h}{\lambda} \approx 0.038\,\frac{m^2K}{W}. \tag{5.5}$$

Now it is possible to estimate the surface temperature T_W of the plate. Assuming a fuel/air mixture temperature $T_0 = 300\,\mathrm{K}$ and an adiabatic flame temperature of $T_{ad} = 2100\,\mathrm{K}$,

$$T_W = T_0 + (T_{ad} - T_0)\frac{R_{\mathrm{fin}}}{R_h + R_{\mathrm{fin}}} \approx 350\,K. \tag{5.6}$$

The temperature of the fuel/air mixture increases slightly as it passes through the perforation. From a simple energy balance one estimates $T_{\mathrm{air}} \approx 325\,\mathrm{K}$. The gas inlet temperature has been set to this value.

Note that heat transfer by radiation has been neglected. The low surface temperature

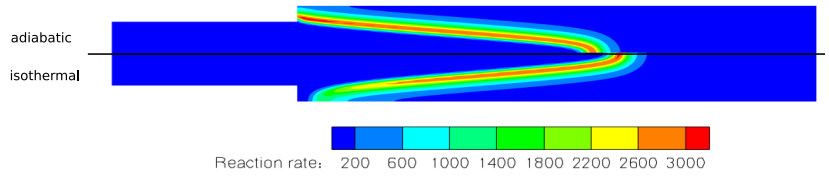

FIGURE 8. Comparison of the position of the flame (reaction rate) for an adiabatic (top) and isothermal (350K) (bottom) wall at the front of the plate

T_W (and the low emissivity of stainless steel, which the plate is made of) justify this simplification. Inside the porous plate, an adiabatic wall boundary condition is imposed.

For "Plate 1" with thickness $l = 3\,\text{mm}$ and fin parameter $\mu = 0.18$ a noticeably higher wall temperature $T_W \approx 600\,\text{K}$ is estimated.

6. Results

The distributions of heat release rate obtained with adiabatic vs. isothermal ($T_W = 350\,\text{K}$) boundary conditions for the porous plate are compared in Fig. 8. As expected, if there is no heat loss to the plate, the flame attaches to the front of the plate. For the isothermal case, there is a stand-off distance of about 1 mm, because the cold wall quenches the reactions close to the wall. This influences the flame dynamics noticeably (see below). A third computation with $T_W = 600\,\text{K}$ gave results quite similar to the ones obtained with 350 K (not shown). Hence, the rough estimate of the temperature outlined in the previous section appears justified.

6.1. *Flame-transfer functions*

Flame-transfer functions obtained from correlation analysis by inversion of the Wiener-Hopf equation (Polifke *et al.* 2001; Gentemann *et al.* 2004) are shown in Fig. 9. Comparing FTFs obtained with adiabatic and isothermal boundary conditions, respectively, one notices a slight difference in phase, and an interesting qualitative difference for the gain: With adiabatic boundary conditions, the gain does not show the characteristic "overshoot" in amplitude $|F(\omega)| > 1$ frequently observed and discussed, e.g., by Birbaud *et al.* (2006). Equation (4.1) suggests that an overshoot in gain is possible if there is interaction of two (or more) dynamic mechanisms. For the present configuration, this could be flame front kinematics, and interaction between heat release and heat transfer at the flame tip (see Rook *et al.* 2002). Obviously, if the flame attaches to the plate, this second interaction mechanism would be suppressed, explaining the monotonous decay of gain observed in that case.

Comparing against experiment, excellent agreement for the phase is observed, while the gain is under-predicted. This could be due to a number of factors: thermal boundary conditions, global kinetic mechanism, fully vs. partly developed flow profile for the flow through the plate, etc. This was not investigated further in this study.

6.2. *Response functions*

The acoustic response H of the CFD model, evaluated at a monitor plane 2 mm upstream of the outlet of the perforation (the "cut" of the CNN setup), is shown in Fig. 10. As one might expect after the discussion in Sec. 4.3, the response shows a prominent peak in gain for frequencies around 500 to 600 Hz, where the phase of the flame frequency

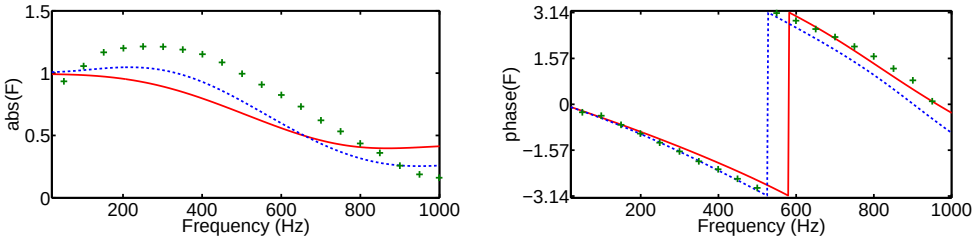

FIGURE 9. Amplitude (left) and phase (right) of the flame transfer functions $F(\omega)$: Computational results obtained with adiabatic (red, solid line) and isothermal (350 K) (blue, dashed line) wall at the front of the plate vs. experimental data of Noiray *et al.* 2007 (+, green). The sign of the phase has been changed to match the sign convention of this work.

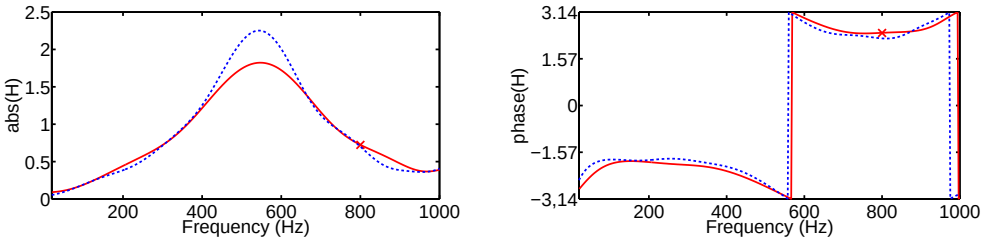

FIGURE 10. Comparison of amplitude (left) and phase (right) of the frequency response function H for an adiabatic (red, solid) and isothermal (350 K) (blue, dashed) wall at the front of the plate. The red "X" marks the result of single frequency harmonic forcing for the adiabatic case.

response F is close to $-\pi$. It is remarkable that the flame frequency response does not have a corresponding local maximum in gain, c.f. Fig. 9.

As discussed previously, the response $H(\omega)$ is computed from one CFD run with broadband excitation by correlation analysis of the resulting time series and subsequent z-transformation of the unit impulse response $\vec{h}$. When doing so, the response $H(\omega)$ can be evaluated for *any* frequency between the minimum frequency $2\pi/N\Delta t$ – where Δt is the sampling interval and N the number of samples – and the Nyquist frequency $\pi/\Delta t$. This is an important improvement over the approach of Kopitz & Polifke (2008), who used superposed sinusoids for excitation and subsequent FFT of time series, resulting in large increments between sampling frequencies and non-smooth Nyquist curves. To validate the new approach based on correlation analysis and z-transform, a sample calculation with single-frequency forcing at 800Hz has been performed. The frequency response was then obtained from the harmonic time series using FFT. The result coincides perfectly with the curve obtained with correlation analysis (see Fig. 10).

6.3. *Stability map*

Eigenfrequencies computed with CNN using the response function H from isothermal CFD with $T_W = 350\,\mathrm{K}$ and the network model for the porous plate as summarized by Eq. (4.2) gave correct predictions of the frequencies. However, the growth rates obtained were in general too large, i.e., the model predicted instability for values of the plenum length L, where stable behavior was observed in experiment. The instable frequencies of the model were between 350 and 650 Hz, corresponding to duct lengths L between 0.09 m and 0.35 m for the first, 0.3 m and 0.75 m for the second and 0.6 m and 0.75 m for the third mode. In contrast, the experiments shows unstable modes at frequencies at 500 -

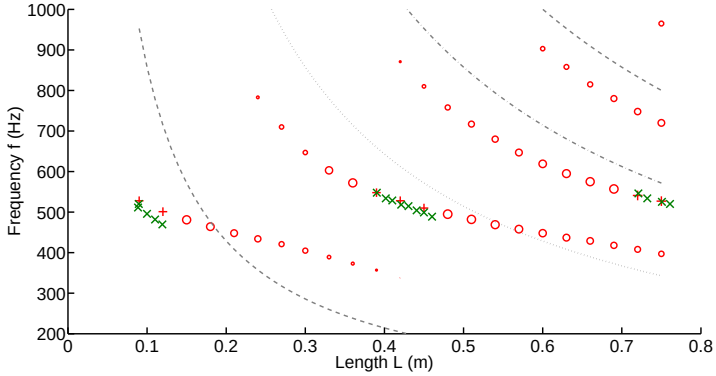

FIGURE 11. Stability map of the perforated plate burner ("Plate 4" with $l = 30\,\text{mm}$): frequencies and growth rates of the first four eigenmodes vs. plenum length. Unstable modes observed in experimental values: "x", CNN from isothermal calculation with $T_W = 350\,\text{K}$ and pressure-loss coefficient $\zeta = 42$: "o" for stable, "+" for unstable modes. The size of the marker indicates the magnitude of the growth/decay rate. Dashed lines correspond to the first quarter-wave modes of the plenum.

600 Hz. The advanced low-order models for the plate described in Sec. 4.4 did not bring significant improvement. Increasing the value of the loss coefficient ζ for the area-change to $\zeta = 42$ (instead of $\zeta = 6$) yields results in good agreement with experiment (see Fig. 11): Instabilities are observed for frequencies in a range from 500 - 600 Hz, coupling with the quarter-wave modes of the plenum. Note that this frequency range corresponds to the maximum overshoot in the response function $H(\omega)$ (see Fig. 10).

The required "tuning" of the loss coefficient ζ implies that the low-order model does not describe the loss mechanisms for acoustic energy at the perforated plate correctly. More accurate models for acoustic wave attenuation in low-Re flow at a perforated plate are obviously required. The work of Rott (1969) could be a starting point for such studies.

7. Summary and conclusions

The thermo-acoustic stability of a laminar premix perforated plate burner was mapped with the novel CNN approach, which combines CFD and a low-order network model to generate a Nyquist plot, from which frequencies and growth rates of both stable and unstable eigenmodes are deduced. Excellent agreement with experiment could be achieved once the pressure-loss coefficient ζ for the flow contraction into the perforated plate was suitably adjusted. It is concluded that more accurate low-order models for wave scattering and attenuation at a perforated plate must be identified.

Due to resonant amplification, the response $H(\omega)$ of plate and flame to incoming acoustic perturbations – represented by the CFD submodel in the CNN context – can have a prominent peak in a fairly narrow frequency range, even though the flame frequency response $F(\omega)$ is not particularly large and monotonously decaying in that frequency range. This phenomenon is significant for the CNN approach, as it can lead to nonlinear response and even divergence of the CFD computation if broad-band forcing with flat power density distribution is applied. It is also significant for experiment – combustion instabilities observed occur in the frequency range where the response is maximal.

Corresponding observations were made previously by Gentemann & Polifke (2007). Consequences for singularity of the OLTF could not be explored fully in this study.

8. Acknowledgements

Financial support from Deutsche Forschungsgemeinschaft (DFG Po 710/03) is gratefully acknowledged. The AVBP solver was made available by CERFACS. Franck Nicoud helped with implementation of isothermal boundary conditions in AVBP, Stephan Föller carried out computations and correlation analysis for the acoustic pressure-loss coefficient and virtual length of the area change. Computations were preformed on the HLRB II at Leibniz Rechenzentrum in Garching, Germany.

REFERENCES

Baade, P. K. 1974 Selbsterregte Schwingungen in Gasbrennern. *Kälte, Klima, Ingenieur* **6**, 167–176.

Birbaud, A. L., Durox, D. & Candel, S. 2006 Upstream flow dynamics of a laminar premixed conical flame submitted to acoustic modulations. *Combustion and Flame* **146** (3), 541–552.

Gentemann, A. & Polifke, W. 2007 Scattering and generation of acoustic energy by a premix swirl burner. In *Int'l Gas Turbine and Aeroengine Congress & Exposition*. May 14 - 17, Montreal, Quebec, Canada.

Gentemann, A. M. G., Hirsch, C., Kunze, K., Kiesewetter, F., Sattelmayer, T. & Polifke, W. 2004 Validation of flame transfer function reconstruction for perfectly premixed swirl flames. In *Int'l Gas Turbine and Aeroengine Congress & Exposition*. June 14 - 17, Vienna, Austria.

Huber, A. & Polifke, W. 2009 Identification of practical premixed flame dynamics by transient CFD and correlation analysis, part I: Theory and proof of concept. *Int. J. of Spray and Combustion Dynamics* submitted .

Kaess, R., Huber, A. & Polifke, W. 2008 A time-domain impedance boundary condition for compressible turbulent flow. In *14th AIAA/CEAS Aeroacoustics Conference (29th AIAA Aeroacoustics Conference)*. AIAA/CEAS, May 5 - 7, Vancouver, Canada.

Kopitz, J. & Polifke, W. 2008 CFD-based application of the Nyquist criterion to thermo-acoustic instabilities. *J. Comp. Phys* **227**, 6754–6778.

Lieuwen, T. & Yang, V., ed. 2006 *Combustion Instabilities in Gas Turbine Engines: Operational Experience, Fundamental Mechanisms, and Modeling*. *Progress in Astronautics and Aeronautics*. ISBN 156347669X. AIAA.

Noiray, N. 2007 Analyse linéaire et non-linéaire des instabilités de combustion, application aux systèmes à injection multipoints et stratégies de contrôle. PhD thesis, École Centrale Paris.

Noiray, N., Durox, D., Schuller, T. & Candel, S. 2007 Passive control of combustion instabilities involving premixed flames anchored on perforated plates. *Proceedings of the Combustion Institute* **31** (1), 1283–1290.

Noiray, N., Durox, D., Schuller, T. & Candel, S. 2008 A unified framework for nonlinear combustion instability analysis based on the flame describing function. *J. Fluid Mech.* accepted .

Polifke, W. 2004 Combustion instabilities. In *Advances in Aeroacoustics and Applications*. Brussels, BE: Von Karman Institute.

Polifke, W. 2007 System modelling and stability analysis. In *Basics of Aero-Acoustics and Thermo-Acoustics*. Brussels, BE: Von Karman Institute.

Polifke, W., Paschereit, C. O. & Sattelmayer, T. 1997 A Universally Applicable Stability Criterion for Complex Thermoacoustic Systems. In *18. Deutsch-Niederländischer Flammentag,* VDI Bericht, pp. 455–460. Delft, NL.

Polifke, W., Poncet, A., Paschereit, C. O. & Döbbeling, K. 2001 Reconstruction of acoustic transfer matrices by instationary computational fluid dynamics. *J. of Sound and Vibration* **245** (3), 483–510.

Polifke, W., Wall, C. & Moin, P. 2006 Partially reflecting and non-reflecting boundary conditions for simulation of compressible viscous flow. *J. of Comp. Phys.* **213** (1), 437–449.

Rook, R., de Goey, L. P. H., Somers, L. M. T., Schreel, K. & Parchen, R. 2002 Response of burner-stabilized flat flames to acoustic perturbations. *Combustion Theory and Modelling* **6**, 223–242.

Rott, N. 1969 Damped and thermally driven acoustic oscillations in wide and narrow tubes. *Z. für Angewandte Mathematik und Physik (ZAMP)* **20** (2), 230–243.

Sattelmayer, T. & Polifke, W. 2003*a* Assessment of methods for the computation of the linear stability of combustors. *Combust. Sci. and Techn.* **175** (3), 453–476.

Sattelmayer, T. & Polifke, W. 2003*b* A novel method for the computation of the linear stability of combustors. *Combust. Sci. and Techn.* **175** (3), 477–498.